no statistically significant difference between the single and multimode mean velocity results. Furthermore, data rates without the etalon and the laser operation at 2.0 W were typically on the order of several thousand per second compared to less than one thousand per second in the case of single-mode operation at 1.2 W (with comparable photomultiplier voltage and signal conditioner amplification).

The velocity fluctuation intensity (the rms level divided by the measured mean velocity) is shown in Fig. 2 for selected conditions. (Again, for clarity, all of the available data were not plotted in this figure.) For both single and multimode operation, it was found that the measured intensity decreased as the filter bandwidth was tightened about the Doppler frequency and as the laser power was increased. These trends are present in the representative data shown in Fig. 2. This behavior was expected.

Comparing single and multimode operation, the single-mode intensities generally showed more sensitivity to laser power. More significantly, the multimode intensities were generally lower than those obtained with tuned etalon, single-mode selection, although the difference between the two was frequently only slightly beyond the limits for statistical significance. These results were not expected.

Dopheide and Durst[1] demonstrated (using a He-Ne laser) that LDA signals containing several beat frequencies have the appearance of noisy signals. One would expect such signals to yield larger "effective" velocity fluctuation intensities and/or reduced data rates due to the presence of additional zero crossings in the high-passed signal. Neither was found to occur in the reported tests, particularly when the additional available laser power was utilized for the multimode tests.

A better understanding and explanation of these test results would require more extensive and systematic testing; however a speculative explanation is proposed: For multimode operation, part of the "noise" in the LDA signal is really the superposition of many higher-frequency beat signals with the Doppler frequency. Theoretically, and other things being equal, single-mode operation should result in an increase in the signal-to-noise ratio (SNR). However, for the reported tests the theoretical gain in SNR may have been entirely offset by the attendant decrease in available laser power. Since the powers reported here were measured on all transmitted wavelengths rather than on the 514.5-nm wavelength alone, and since the power available in the 514.5-nm line depends upon which axial mode is selected during etalon tuning, it is likely that the actual power available was significantly lower for the single-mode tests. In addition, spectral analysis[1] shows that the power in the beat frequencies is lower than the power at the Doppler frequency and, in the present case, many beat frequencies did not contribute to the "noise" since electronic filtering conveniently removed all but one. As a consequence, it is possible that the actual SNR was higher in multimode tests at 1.0 and 2.0 W than in the single-mode tests at 1.2 W. This would be consistent with the improved data rate and lower velocity fluctuation intensities found using the multiaxial-mode laser.

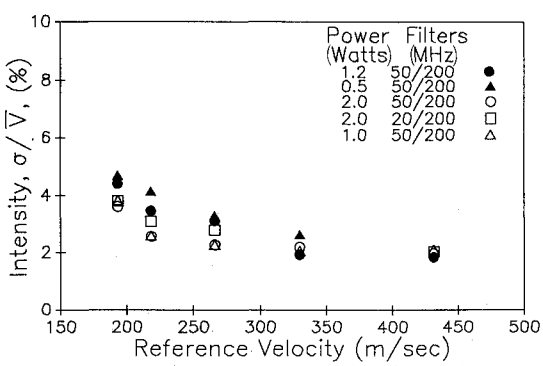

Fig. 2 Measured turbulence intensity (%) vs tunnel reference velocity. Open symbols, multimode operation; solid symbols, single-mode operation.

Conclusions

The results of these tests indicate that the presence of beat frequencies in the LDA signal does not necessarily result in poor quality measurements or reduced data rate. In particular, no effect was observed in the mean velocity measurements, and the data rates for multimode operation exceeded single-mode data rates when the additional beam power was employed. Higher-level velocity fluctuation intensities were not associated with multimode operation.

Reference

[1]Dopheide, D., and Durst, F., "High Frequency Laser Doppler Measurements Using Multiaxial-Mode Lasers," *Applied Optics*, Vol. 20, No. 9, 1981, pp. 1557-1570.

Induced Drag of a Wing in a Circular Wind Tunnel

Yuzo Yamamoto*
Gifu National College of Technology, Motosu, Gifu, Japan

Nomenclature

b	= wing span
E	= complete elliptic integral of the second kind, modulus k
e	= span efficiency factor, $C_{Di} = C_L^2/(\pi A_R e)$
K	= complete elliptic integral of the first kind, modulus k
k	= modulus of elliptic function, $\lambda^2 = (b/d)^2$
sn v, cn v, dn v	= Jacobian elliptic functions, modulus k
v	= variable, modulus k, $x = \text{sn } v$
W	= uniform downwash
w	= downwash on wing vortex trace
$Z(v)$	= Jacobian theta function, modulus k, $E(v) - (E/K)v$
Γ	= bound vortex circulation
γ	= trailing vortex strength
ϵ	= clearance between wing tip and wind-tunnel boundary to wind-tunnel radius ratio, $1 - (b/d)$
Subscripts	
c	= closed-tunnel case
0	= open-tunnel case

Introduction

In our previous paper,[1] the exact expression of the spanwise optimum lift distribution and the minimum induced drag of a straight wing in a circular closed wind tunnel have been obtained from the Trefftz plane flowfield analysis. In this study, the spanwise optimum lift distribution and minimum induced drag of a wing in a circular wind tunnel, with either a closed or an open working section, are examined exactly. In the closed-tunnel case, an alternative analysis with Ref. 1 is derived, and the lift distribution and the induced drag that are obtained by the present analysis are coincident with those of Ref. 1. In the Trefftz plane flowfield analysis, the method of

Received April 8, 1991; revision received Sept. 5, 1991; accepted for publication Oct. 20, 1991.

*Professor, Department of Mechanical Engineering.

Ref. 1 used a comformal mapping and Söhngen's inversion integral formula,[2] but the method of this study directly uses Söhngen's formula through an independent variable transformation. In the open-tunnel case, the exact solutions of the minimum induced drag and the optimum spanwise lift distribution are found. Throughout this Note the flow is assumed inviscid and incompressible.

The most important configuration parameter is the wing span to tunnel diameter ratio b/d. For conventional wind-tunnel tests, this ratio may be 7/8 or less, where many useful theories are available.[3-6] However, useful theoretical works cannot be found except Ref. 1, which treats the closed-tunnel case only, if the ratio b/d is approached to unity. For the open-tunnel case, this Note shows a useful theory that is valid in the whole b/d range $0 \le b/d \le 1$.

Closed-Tunnel Case

Consider the Trefftz plane flowfield, then the relation of normal downwash w_c and trailing vortex γ_c is

$$w_c(x) = \frac{1}{2\pi} \int\!\!\!\!\!\!-_{-1}^{1} \gamma_c(x_1) \left[\frac{1}{x_1 - x} - \frac{1}{(1/\lambda^2 x_1) - x} \right] dx_1 \qquad (1)$$

When a new independent variable η is introduced by a relation

$$\lambda x + [1/(\lambda x)] = [\lambda + (1/\lambda)]/\eta$$

Söhngen's inversion integral formula[2] could be adapted to Eq. (1), and the the following expression is obtained:

$$\frac{x}{\eta}\gamma_c(\eta) = -\frac{2}{\pi} \int\!\!\!\!\!\!-_{-1}^{1} \sqrt{\frac{1-\eta_1^2}{1-\eta^2}} \frac{(x_1/\eta_1) w_c(\eta_1)}{\eta_1 - \eta} d\eta_1 + \frac{C_1}{\sqrt{1-\eta^2}} \qquad (2)$$

The wing bound vortex circulation $\Gamma(x)$ is given by

$$\tilde{\Gamma}(x) = \int_x^1 \gamma(x)\, dx$$

where $\tilde{\Gamma}(x) = \Gamma(x)/[b/2]$.

In the minimum induced drag case,

$$w(x) = \text{const} = W$$

and the span efficiency factor e is as follows:

$$e = [1/(\pi W)] \int_{-1}^{1} \tilde{\Gamma}(x)\, dx$$

where

$$C_{Di}(\text{optimum}) = C_L^2/(\pi A_R e)$$

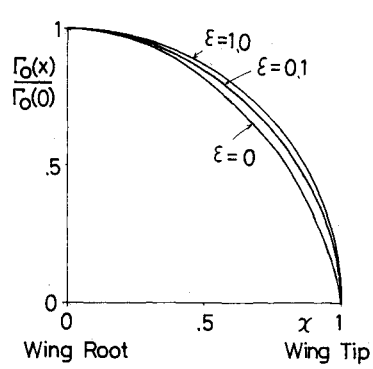

Fig. 1 Open-wind tunnel case spanwise optimum lift distribution shape and ϵ.

Jacobian elliptic functions[7] are introduced and the spanwise optimum lift distribution expression is obtained, which is an alternative form of Eq. (13) in Ref. 1:

$$\tilde{\Gamma}_c(v) = \frac{4W}{\pi} \left[K \operatorname{cn} v \operatorname{sn} v + \left(\operatorname{sn} v + \frac{1}{k \operatorname{sn} v} \right) KZ(v) \right] \qquad (3)$$

When the wing span to tunnel diameter ratio b/d reaches zero, the approximate solution of the spanwise optimum lift distribution shape is as follows:

$$\left.\frac{\Gamma_c(x)}{\Gamma_c(0)}\right|_{b/d \to 0} = \sqrt{1-x^2} + \frac{k^3}{8} x^2 \sqrt{1-x^2} + \mathcal{O}(k^4)$$

If the b/d ratio reaches unity, the approximate solution of the spanwise optimum lift distribution shape is

$$\left.\frac{\Gamma_c(x)}{\Gamma_c(0)}\right|_{b/d \to 1} = 1 + \frac{1}{\ell n(1/\epsilon) + 2\ell n 2 - 1} \times \left[1 - \tfrac{1}{2} \left(x + \frac{1}{x} \right) \ell n \frac{1+x}{1-x} \right] + \mathcal{O}(\epsilon)$$

See Fig. 3 in Ref. 1, which shows the relation of the closed-tunnel case optimum lift distribution shape to gap width ratio ϵ.

The following span efficiency factor in the minimum induced drag case is obtained:

$$e_c = \frac{4}{\pi^2 k} \left\{ (1+k)^2 K^2 - \frac{[(1+k)K - E]^2}{k} \right\} - \frac{1}{k} \qquad (4)$$

When the wing span to tunnel diameter ratio b/d reaches zero, the approximate solution of e_c is as follows:

$$\left. e_c \right|_{b/d \to 0} = 1 + \frac{k}{2} + \frac{k^2}{4} + \frac{7}{32} k^3 + \frac{5}{32} k^4 + \mathcal{O}(k^5)$$

If the b/d ratio reaches unity, the approximate solution of e_c is

$$\left. e_c \right|_{b/d \to 1} = \frac{4}{\pi^2} \left[2\ell n \frac{1}{\epsilon} + 4\ell n 2 - 1 - 6(\ell n 2 - 1)\epsilon \ell n \frac{1}{\epsilon} \right] - 1 + \mathcal{O}(\epsilon)$$

The relation of e_c to ϵ has been shown in Fig. 4 in Ref. 1.

Open-Tunnel Case

A following open-tunnel case spanwise optimum lift distribution is obtained in the present study:

$$\tilde{\Gamma}_0(v) = (4W/\pi)[K \operatorname{cn} v \operatorname{dn} v + \{\operatorname{sn} v - [1/(k \operatorname{sn} v)]\} KZ(v)] \qquad (5)$$

When b/d reaches zero, the approximate solution of the open-tunnel case spanwise optimum lift distribution shape is as follows:

$$\left.\frac{\Gamma_0(x)}{\Gamma_0(0)}\right|_{b/d \to 0} = \sqrt{1-x^2} - \frac{k^3}{8} x^2 \sqrt{1-x^2} + \mathcal{O}(k^4)$$

If b/d reaches unity, the asymptotic solution is

$$\left.\frac{\Gamma_0(x)}{\Gamma_0(0)}\right|_{b/d \to 1} = \frac{1}{2} \left(\frac{1}{x} - x \right) \ell n \frac{1+x}{1-x} + \epsilon \ell n \left(\frac{1}{\epsilon} \right) + \mathcal{O}(\epsilon)$$

The relation of the open-tunnel case spanwise optimum lift distribution shape $\Gamma_0(x)/\Gamma_0(0)$ to ϵ is examined and shown in Fig. 1.

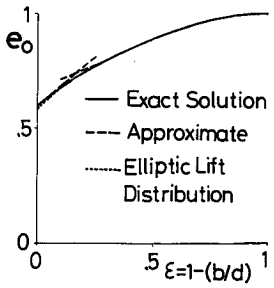

Fig. 2 Open-tunnel case span efficiency factor e_0 vs ϵ.

A following open-tunnel case span efficiency factor in the minimum induced drag is obtained:

$$e_0 = \frac{8}{\pi^2}\left[\frac{k-1}{2k^2}(1-k^2)K^2 + \frac{1-k}{k^2}KE - \frac{E^2}{2k^2}\right] + \frac{1}{k} \qquad (6)$$

When b/d reaches zero, the approximate solution of e_0 is

$$e_0\Big|_{b/d\to 0} = 1 - \frac{k}{2} + \frac{k^2}{4} - \frac{7}{32}k^3 + \frac{5}{32}k^4 + \mathcal{O}(k^5)$$

If b/d reaches unity, the approximate solution of e_0 is

$$e_0\Big|_{b/d\to 1} = 1 - (4/\pi^2) + 2\epsilon[1 - (4/\pi^2)]$$

The relation of the open-tunnel case span efficiency factor e_0 to ϵ is examined by high-speed digital computer and shown in Fig. 2.

Conclusions

The closed forms of both the spanwise optimum lift distribution and the minimum induced drag in the closed-tunnel case are obtained, and the results are coincident with those of our previous paper. Open-tunnel case explicit expressions of both the spanwise optimum lift distribution and the minimum induced drag are obtained.

Appendix: Elliptic Spanwise Lift Distribution Wing in Closed or Open Wind Tunnel

The span efficiency factor of a wing in a circular closed or open tunnel e_{ellipt} is as follows[4]:

$$e_{\text{ellipt}} = \frac{1}{1 \mp [4/(\pi k)]\,[(\pi/2) - E]} \qquad (A1)$$

where the $-$ sign of the double sign $\mp$ indicates the closed-tunnel case and the $+$ sign indicates the open-tunnel case.

The asymptotic solutions for $b/d \to 0$ are

$$e_{\text{ellipt}} = 1 \pm \frac{k}{2} + \frac{k^2}{4} \pm \frac{7}{32}k^3 + \frac{5}{32}k^4 + \mathcal{O}(k^5) \qquad (A2)$$

where the $+$ sign of each double sign $\pm$ indicates the closed-tunnel case and the $-$ sign indicates the open-tunnel case.

The limiting values at $b/d \to 1$ are

$$e_{\text{ellipt}_{b/d=1}} = \frac{1}{1 \mp [2 - (4/\pi)]} \qquad (A3)$$

where the $-$ sign of the double sign $\mp$ indicates the closed-tunnel case and the $+$ sign indicates the open-tunnel case.

Acknowledgment

The author would like to express his appreciation to S. Ando.

References

[1]Ando, S., and Yamamoto, Y., "Induced Drag of a Straight Wing in a Wind Tunnel of Circular Cross Section," *Ingenieur Archiv*, Bd. 45, H. 3, 1976, pp. 161-170.

[2]Bisplinghoff, R. L., Ashely, H., and Halfman, R. L., *Aeroelasticity*, Addison-Wesley, Cambridge, MA, 1955, p. 217.

[3]Rosenhead, L., "The Effect of Wind Tunnel Interference on the Characteristics of an Aerofoil," *Proceedings of the Royal Society of London, Series A*, Vol. 129, Nov. 1930, pp. 135-145.

[4]Moriya, T., *Introductions to Aerodynamnics*, in Japanese, Baifukan, Tokyo, 1959, pp. 233-238.

[5]Millikan, C. B., "On the Lift Distribution for a Wing of Arbitrary Plane Form in a Circular Wind Tunnel," *Transactions of the ASME, Journal of Applied Mechanics*, APM-54-19, 1932, pp. 197-203.

[6]Rae, W. H., Jr., and Pope, A., *Low-Speed Wind Tunnel Testing*, 2nd ed., Wiley, New York, 1984, pp. 376-383.

[7]Byrd, P. F., and Friedman, M. D., *Handbook of Elliptic Integrals for Engineers and Scientists*, 2nd ed., Springer-Verlag, Berlin, 1971.

Qualitative Model for Visualizing Shock Shapes

Masatomi Nishio*
Fukuyama University, Fukuyama 729, Japan

I. Introduction

THE visualization of three-dimensional shock shapes using electric discharge was previously attempted.[1] However, we did not know reasonable theory of the visualization. Therefore, it has been difficult to select suitable experimental conditions. Consequently, the visualization of shock shapes has been difficult and they have not been visualized very successfully. A qualitative theory of the visualization has now been established by considering the relation among the radiation intensity from the electric discharge, the excitation function vs electron energies, and the gas molecular number density. Applying this qualitative theory of the visualization, it was found that there exists the most suitable experimental condition. Utilizing this knowledge, it has become easy to visualize three-dimensional shock shapes.

II. Visualizing Principle

In general, excitation functions rise according to the increase of electron energies and, once they have reached their maximums, decline according to the increase of electron energies. As mentioned by Nasser,[2] the decline in all types of excitation functions after reaching the maximums can be explained purely qualitatively by considering the actual collision process that can be visualized by considering the interaction of the electromagnetic fields of the two colliding particles. When the oncoming particle is a fast electron "wave," the period of interaction of the fields of the waves of both particles become very short. The amount of kinetic energy and momentum transferred from the electron to the molecule also decreases. Hence, if the electron is too fast no "collision" takes place, as no appreciable interaction of fields is effective in the short time.

Radiation intensity I from an electric discharge is proportional to the product of the excitation function F and the gas molecular number density N. Because the excited molecule's electron, upon resuming stability, discharges light in an amount equal to its excitation energy, and because the number

Received Sept. 17, 1991; revision received Jan. 22, 1992; accepted for publication Feb. 10, 1992.

*Associate Professor, Department of Mechanical Engineering. Member AIAA.